ISSN 0016-7932, Geomagnetism and Aeronomy, 2022, Vol. 62, No. 3, pp. 199–208. © Pleiades Publishing, Ltd., 2022.
Russian Text © The Author(s), 2022, published in Geomagnetizm i Aeronomiya, 2022, Vol. 62, No. 3, pp. 325–335.

Global Development of the Supersubstorm of May 28, 2011

I. V. Despirak[a], *, N. G. Kleimenova[b], A. A. Lyubchich[a], P. V. Setsko[a], L. I. Gromova[c], and R. Werner[d]

[a] *Polar Geophysical Institute, Apatity, Murmansk oblast, Russia*
[b] *Shmidt Institute of Physics of the Earth, Russian Academy of Sciences, Moscow, Russia*
[c] *Pushkov Institute of Terrestrial Magnetism, Ionosphere, and Radiowave Propagation, Russian Academy of Sciences, Troitsk, Moscow, Russia*
[d] *Space Research and Technology Institute, Bulgarian Academy of Sciences, Stara Zagora, Bulgaria*
**e-mail: despirak@gmail.com*

Received December 7, 2021; revised January 20, 2022; accepted January 27, 2022

Abstract—The paper gives an analysis of the isolated supersubstorm observed during the main phase of the moderate magnetic storm on May 28, 2011 ($SYM/H \sim -95$ nT), which was caused by the solar wind magnetic cloud. This supersubstorm peaked at around ~0850 UT ($SML = \sim -2600$ nT). The study was based on data from the global SuperMAG and IMAGE magnetometer networks and satellite data from the AMPERE project. Like those in other supersubstorms, the ionospheric currents in this event were found to develop on a global scale: an intense and extended westward electrojet (with a maximum around midnight) was observed in the midnight, morning, and daytime sectors and an intense eastward electrojet was observed in the afternoon and evening sectors. The development of global currents was accompanied by intense positive bays. This was reflected by large values of the *MPB* index (~4000 nT^2). It has been shown that, during the peak development of the supersubstorm, there was a significant increase in the eastward electrojet in the evening sector (~15–18 MLT), an additional affluent longitudinal electric current, and an additional ring current that appeared concurrently in this sector. These facts suggest the hypothesis about the development of an additional substorm current wedge that appeared on the evening side during the supersubstorm and closed on the eastward electrojet.

DOI: 10.1134/S0016793222030069

1. INTRODUCTION

Supersubstorms (SSSs) are intense substorms with large negative values of the *SML* index ($SML < -2500$ nT) (Tsurutani et al., 2015). Unlike the *AL* index, the *SML* index is calculated from observational data from the SuperMAG global network of stations (Gjerloev, 2009, 2012; Newell and Gjerloev, 2011) and, therefore, includes not only the standard stations of the auroral zone (which is characteristic of the *AL* index) but also many other stations (from 40° to 80° MLAT). This is important for studies of intense substorms, during which geomagnetic activity can strongly shift in latitude (Feldstein and Starkov, 1967).

The first studies indicated that SSSs have some features both in space weather conditions during the appearance of SSSs and in the development of ground-based geomagnetic disturbances at this time. According to Despirak et al. (2019, 2020) and Hajra et al. (2016), SSSs are observed only under certain conditions in the solar wind: namely, the passage of magnetic clouds (MCs) or regions of compressed plasma in front of magnetic clouds (SHEATH), when there are jumps in the solar-wind pressure and large negative values of the B_Z components of the interplanetary magnetic field (IMF). In general, these conditions are also characteristic of the development of large magnetic storms. However, SSS events are not always associated with intense magnetic storms, as it would be logical to assume; they can also be observed during moderate magnetic storms and sometimes under nonstorm conditions (Despirak et al., 2019; Tsurutani et al., 2015).

Until now, detailed studies of SSS development have been performed only for a few events: September 8, 2017; March 9, 2012; and April 5, 2010 (Despirak et al., 2020, 2021; Haira et al., 2018; Nishimura et al., 2020; Zong et al., 2021). An analysis of the SSS development during the moderate storm on April 5, 2010, showed that this supersubstorm was characterized by some special features: an extremely intense magnetic reconnection, an unusually large dipolization, and intense fast plasma streams directed towards the Earth (which were observed by the THEMIS-A and GOES-11 satellites) (Nishimura et al., 2020). IMAGE satellite observations indicated that, unlike the situation with classical substorms (Akasofu, 1964), intense auroras were observed in the premidnight and morning sectors of magnetic local time (MLT) in this case (Hajra et al., 2018). In addition, this supersubstorm was found to be characterized by an unusual spatial pattern of the

development of auroral electrojets: both (eastward and westward) electrojets developed globally and surround the polar cap from different sides to reach the day side. As a result, a complex, layered pattern of field-aligned currents and corresponding ground-based magnetic bays formed. It was recorded on the meridian of the IMAGE magnetometer network.

All of the supersubstorm events analyzed here (both the SSS of April 5, 2010, and the events of September 8, 2017, and March 9, 2012) were characterized by some features in the planetary distribution of electrojets. The main feature is the formation of a strong westward electrojet on a global scale from the evening side at auroral latitudes to the dayside in the polar region (Despirak et al., 2020, 2021). It is quite probable that the daytime polar disturbances observed simultaneously with nighttime supersubstorms are caused by the leakage of the westward electrojet onto the day side (Feldstein et al., 2006).

It is known that the westward electrojet is part of a substorm current wedge (SCW). This refers to a three-dimensional system of currents that arises normally on the night side due to a current disruption near the geosynchronous orbit, when the current across the plasma sheet of the magnetosphere closes on the ionosphere through field-aligned electric currents (Meng and Akasofu, 1969; McPherron et al., 1973). In this case, the westward electrojet closes by a pair of downward and upward field-aligned currents, which are separated azimuthally; as a result, positive deviations (positive bays) are created in the *H* component at middle and low latitudes (Chu et al., 2014; Connors et al., 2014; Rostoker, 1968). A midlatitude *MPB* index was recently proposed to estimate the SWC intensity (McPherron and Chu, 2017; Chu et al., 2015). This index is calculated from SuperMAG magnetometer data as the average power of variations in the *X* and *Y* components of the magnetic field at midlatitude stations and can serve as a measure of the intensity of midlatitude bays and the intensity of dipolarization during a substorm (Sergeev et al., 2011).

In addition, as noted in our previous work (Despirak et al., 2021), an intense, eastward electrojet developed in the afternoon and evening sectors during the SSS. The strong, eastward electrojet on the evening side may be associated with the formation of an additional ring current in the evening sector during the SSS (Zong et al., 2021). The resulting additional ring current closes through field-aligned currents on the eastward electrojet; i.e., it is assumed that an additional current loop (i.e., an additional substorm current wedge) appears in the evening side during intense substorms or supersubstorms (Fu et al., 2021; Zong et al., 2021).

The goal of the paper is to continue the study of geomagnetic effects and the spatial development of electrojets during supersubstorms and to verify the assumption that an additional current wedge of the opposite direction formed in the pre-evening sector during the SSS, leading to an increase in the eastward electrojet. One of the few isolated events was chosen for analysis: a supersubstorm observed during the moderate magnetic storm on May 28, 2011. This SSS is an isolated event, since it was observed against a quiet background and there were no disturbances in the *SML* index with an intensity exceeding 500 nT. It should be noted that the SSSs considered earlier cases (the events of September 8, 2017, and March 9, 2012) were not isolated; the supersubstorms were observed against a rather disturbed geomagnetic background and consisted of a series of peaks in the *SML* index with an intensity exceeding ~2000 nT.

2. DATA

In this work, we analyze ground-based observations from the global network of SuperMAG magnetometers (http://supermag.jhuapl.edu/) (Gjerloev, 2009; Newell and Gjerloev, 2011). Also, observational data from the IMAGE Scandinavian network of stations (http://space.fmi.fi/image/) (Viljanen and Häkkinen, 1997) were used.

The onset and development of the supersubstorm were determined based on the geomagnetic *SML* index taken from the SuperMAG website and magnetograms. In the SuperMAG system, the magnetic-field components are $B = (B_N, B_E, B_Z)$, where *N* is the direction toward the local magnetic North; *E* is the direction toward the local magnetic East; and *Z* is the vertical downward direction (Gjerloev, 2009, 2012; Newell and Gjerloev, 2011).

The ring-current intensity and distribution over the MLT sectors were determined with the *SMR* and *SMR_LT* indices, which were also taken from the SuperMAG website. The *SMR* index characterizes the ring-current intensity and is calculated from variations in the *N* component of the magnetic field measured by ~100 magnetometers located from −50° to +50° of geomagnetic latitude. In the SuperMAG project, the calculation of magnetic activity indices is based on the identification of four sectors of local time with centers at 00, 06, 12, and 18 MLT, for which the *SMR_LT* value is determined (*SMR-00*; *SMR-06*; *SMR-12*; and *SMR-18*, respectively). The total value of the *SMR* index is then determined from the formula $SMR = (SMR\text{-}00 + SMR\text{-}06 + SMR\text{-}12 + SMR\text{-}18)/4$ (Newell and Gjerloev, 2011).

The intensity of the midlatitude bays was determined from the *MPB* index, which was built from additional material for the electronic version of the paper (McPherron and Chu, 2017). The *MPB* index is calculated from SuperMAG magnetometer data as the average power of variations in the *X* and *Y* components of the magnetic field; here, the sum of the squares of the power of *X* and *Y* is determined at each of 35 midlatitude stations. A detailed description of the meth-

odology for calculation of the *MPB* index and the lists of midlatitude stations can be found in (McPherron and Chu, 2017; Chu et al., 2015).

The global spatial distribution of ionospheric currents was determined from the maps of magnetic field vectors obtained by SuperMAG magnetometers and maps of magnetic disturbances obtained from the results of a spherical harmonic analysis of magnetic measurements on 66 simultaneously operating, low-apogee communication satellites at the altitude of around 780 km by the Active Magnetosphere and Planetary Electrodynamics Response Experiment (AMPERE). A detailed description of the methodology used to obtain these data can be found at http://www.ampere.jhuapl.edu.

The solar-wind and IMF parameters were taken from the CDAWeb database and the catalog of large-scale solar wind types (ftp://ftp.iki.rssi.ru/pub/omni/catalog).

3. RESULTS

3.1. Conditions of the Solar Wind and Interplanetary Magnetic Field

Figure 1 shows the solar-wind and interplanetary magnetic-field (IMF) parameters observed at 02–17 UT on May 28, 2011: the magnitude (B_T) of IMF, the Y and Z components of IMF (B_Y, B_Z), the flow velocity (V), the dynamic pressure (P) of the solar wind, and the geomagnetic indices PC, *SYM/H*, and *SML*.

It can be seen that a coronal mass ejection (CME) was observed near the Earth during this time period (Fig. 1 shows data for a distance of 1 AU). It consisted of two successive structures: SHEATH and a magnetic cloud (MC). The turbulent region of compressed SHEATH plasma with increased density, temperature, and magnetic field was observed from ~04 UT on May 27 to ~0620 UT on May 28, and MC was observed from ~0620 to 2100 UT on May 28. In this figure, the SHEATH and MC regions are shown as horizontal arrows. At the end of the SHEATH region, at around 0300 UT, there was a jump in the solar-wind parameters corresponding to the arrival of a shock wave (*IS*); this time instant is shown in Fig. 1 as a vertical solid line. It follows from Fig. 1 that the MC contains a large interval of negative values of the IMF B_Z component. At around ~0620 UT, the sharp change of the B_Z component of the IMF from +4 to −10 nT began and the B_Z IMF remained negative until ~14 UT, with a minimum value of −13 nT. It was most likely the long period of negative B_Z values that led to the development of a moderate geomagnetic storm with Dst = −95 nT.

Against the background of this magnetic storm, the SSS began to develop with a minimum value of the *SML* index of ~−2500 nT. This SSS began at ~0805 UT (this time instant is marked in Fig. 1 by a vertical

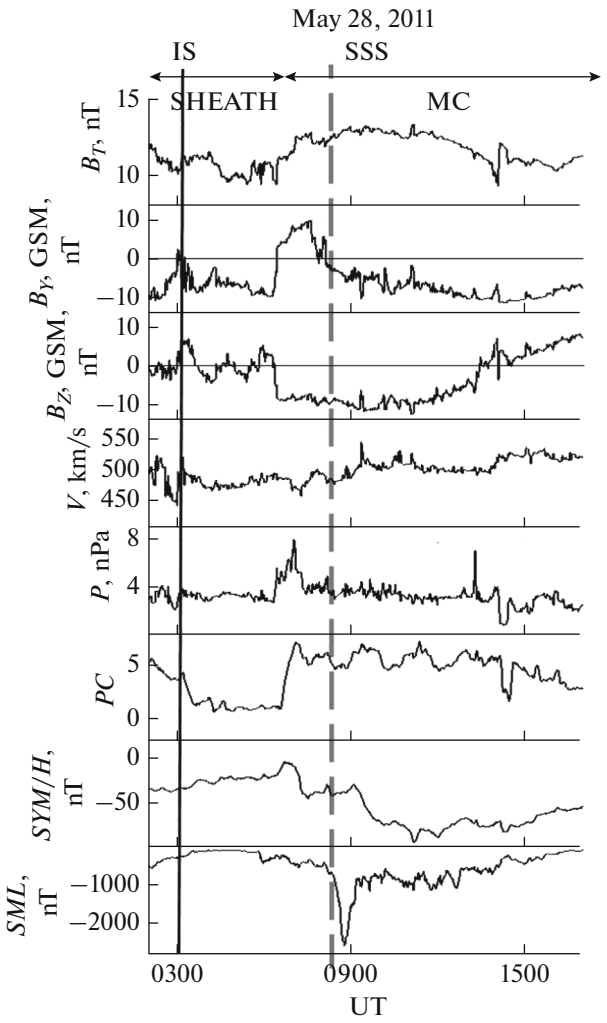

Fig. 1. Parameters of the solar wind and IMF and the geomagnetic indices for 02–17 UT on May 28, 2011. From top to bottom: the IMF magnitude (B_T), B_Y and B_Z components of the IMF (in the GSM system), the velocity and dynamic pressure of the solar wind, and the geomagnetic indices PC, *SYM/H*, and *SML*. The boundaries of the magnetic cloud (MC) and the SHEATH regions are indicated by horizontal arrows, the shock wave arrival (IS), and the SSS onset times are marked by vertical lines (solid and dashed, respectively).

dashed line), reached a maximum at ~0850 UT, and terminated at around 0910 UT on May 28, 2011. Thus, the duration of the SSS was ~1 h. It can be seen that the SSS began at the main phase of the storm (*SYM/H* ~ −50 nT), at the beginning of the MC. Before the SSS, a jump in solar-wind pressure was observed, the B_Z component of IMF was negative, and the B_Y component was positive.

It can be seen from Fig. 1 that the B_Z-component of IMF became negative approximately an hour and a half before the SSS onset, which contributed to the influx of the solar-wind energy into the Earth's magnetosphere. The indicator of this process is known to

Table 1. Geomagnetic coordinates of the SuperMAG stations used in this study

Station	MLAT	MLON	MLT (at 09 UT)
Kaktovik (KAV)	71.5°	–94.7°	22
Barrow (BRW)	70.6°	–106.5°	21
Fort Yukon (FYU)	67.6°	–92.7°	22
College (CMO)	65.4°	–93.8°	22
Yakutsk (YAK)	54.9°	–157.4°	18
Magadan (MGD)	54.3°	–139.3°	19
Paratunka (PET)	46.7°	–132.1°	20

be the polar PC index (Troshichev et al., 2014). Figure 1 shows that the PC index rapidly increased from 1 to 7 before the SSS onset. This indicates the incoming of a very large amount of energy from the solar wind into the Earth's magnetosphere.

3.2. Development of the Supersubstorm from Ground-Based and Satellite Geomagnetic Disturbances

Let us consider the spatial distribution of magnetic disturbances during the SSS of May 28, 2011. Figure 2 shows the distribution maps of magnetic-field vectors obtained from SuperMAG data. The top panel shows the maps for three time instants (0820, 0830, and 0855 UT), which can be used to trace the dynamics of SSS development. In Figure 2a, the magnetic vectors are rotated clockwise by 90° to show the direction of the ionospheric equivalent electric currents. It can be seen from the continental outlines that the stations of Alaska and Canada were located in the premidnight and night sectors, Greenland was located in the morning sector, Siberia and the Far East were located in the evening sector (MLT ~ 16–19 h), and Scandinavia, where the stations of the IMAGE meridional profile are located, was in the daytime sector. It should be noted that the location of magnetic stations is nearly the same as for the case of the SSS of April 5, 2010. It can be seen that the disturbances began in the night sector, in northern Canada; then, they intensified, and the area of their observation expanded, capturing stations in the north of the United States and propagating both westward (towards Alaska and the Far East) and eastward (towards Greenland and Scandinavia). At the SSS-development maximum, the strongest disturbances were observed in the premidnight sector in Alaska (~2000 nT) and in the night sector in southern Canada (~1700 nT). The magnetic vector maps show that the westward electrojet developed on a global scale, from the evening sector (Alaska) through the night (Canada) and morning (Greenland) sectors to the daytime sector (Scandinavia).

Figure 2b shows the magnetograms of some stations in Alaska according to the SuperMAG data (http://supermag.jhuapl.edu/). Variations in the *N* component of the magnetic field are shown at the following four stations in Alaska: Kaktovik (KAV), Barrow (BRW), Fort Yukon (FYU), and College (CMO) from 06 to 11 UT on May 28, 2011. Table 1 gives the geomagnetic coordinates of all stations used in this study. These stations were located in the near-midnight sector; starting from ~0825 UT, strong negative bays (more than ~1000 nT) were observed here. In this case, the strongest disturbances were recorded at the auroral latitudes, at CMO and FYU stations (~–2200 nT).

It is rather difficult to estimate magnetic disturbances in the evening sector due to the sparseness of the network of magnetic stations over the large Siberian region. Figure 2c shows the magnetograms of some stations in Siberia and the Far East obtained according to SuperMAG data. Variations in the *N* component of the magnetic field are shown at the following three stations in Eastern Siberia and the Far East: Yakutsk (YAK), Magadan (MGD), and Paratunka (PET). Table 1 gives the geomagnetic coordinates of these stations. It can be seen that sufficiently intense positive bays were observed at these stations. The largest disturbances (~220 nT) were recorded in the evening sector (~18 MLT) at Yakutsk; the amplitude of the bays decreases from Yakutsk (YAK) to Kamchatka (PET). It should be noted that the amplitudes of positive bays for ordinary substorms are normally much smaller (~20–30 nT) (Guineva et al., 2021). The positive bays indicate the presence of an intense eastward electrojet. However, to draw more reliable conclusions about magnetic disturbances and the positions of electrojets, one should use satellite data from the AMPERE project.

Figure 3 shows the results of the analysis of magnetic disturbances according to measurements conducted by 66 AMPERE satellites at an altitude of 780 km on May 28, 2011. The maps of the spherical harmonic analysis of magnetic disturbances (left) and maps of the distribution of field-aligned currents (right) are shown; the upward and downward currents are marked with circles and crosses, respectively. The maps are built in geomagnetic coordinates for the Northern Hemisphere; noon and midnight are at the top and bottom of the map, respectively. It should be noted that the AMPERE website (http://www.ampere.jhuapl.edu) presents the field-aligned current distribution maps in color: the

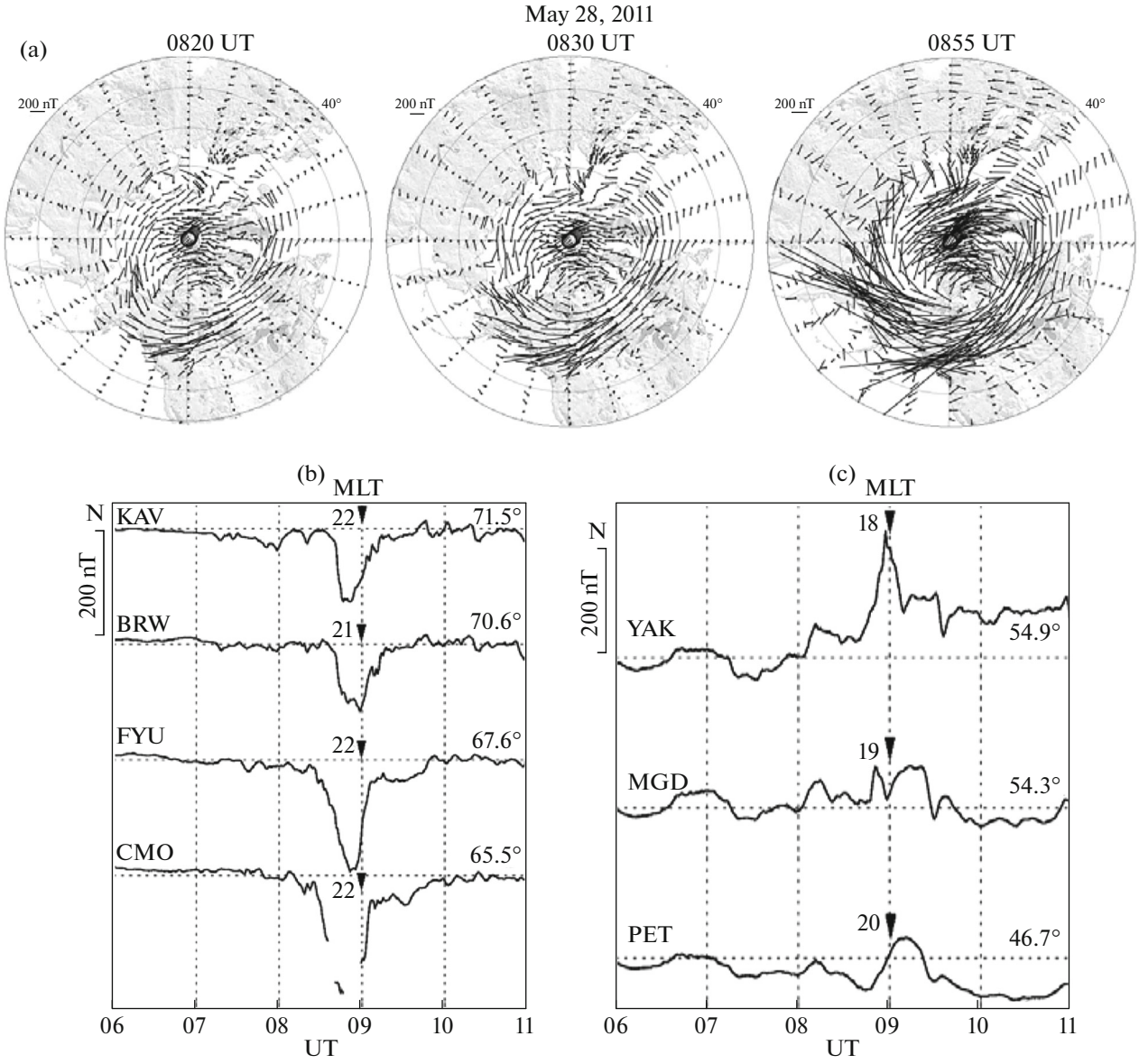

Fig. 2. Observations on the SuperMAG network during the SSS: maps of the spatial distribution of magnetic-field vectors rotated by 90° to show (a) the direction of ionospheric equivalent electric currents and variations in the N component of the magnetic field at individual stations in (b) Alaska and (c) Eastern Siberia and the Far East.

upward currents are in red, and the downward currents are in blue. When color drawings are converted into black-and-white ones, these colors become indistinguishable; therefore, we used special symbols (crosses and circles). However, data on the intensity of currents are completely lost here, and only their position and spatial development can be assessed.

Figure 3 shows the maps for two time instants close to 0830 and 0900 UT, i.e., at the beginning and at the maximum of the SSS development (Figs. 3a and 3b). It can be seen that two extended electrojets were recorded at approximately 0830 UT: the westward electrojet, which was observed from premidnight to late morning hours of local time, and the eastward electrojet, which was observed from noon to late evening hours. The westward electrojet is located between the downward and upward currents, and the eastward one is between the upward and downward currents. It can be seen that the geomagnetic disturbances develop in auroral latitudes in the night sector and in polar latitudes in the morning and daytime sectors.

At the maximum development of the SSS at around 0900 UT, the currents intensified, expanding in latitude; this was especially manifested in the night sector at around midnight, and the downward and upward currents expanded by almost two times. In the

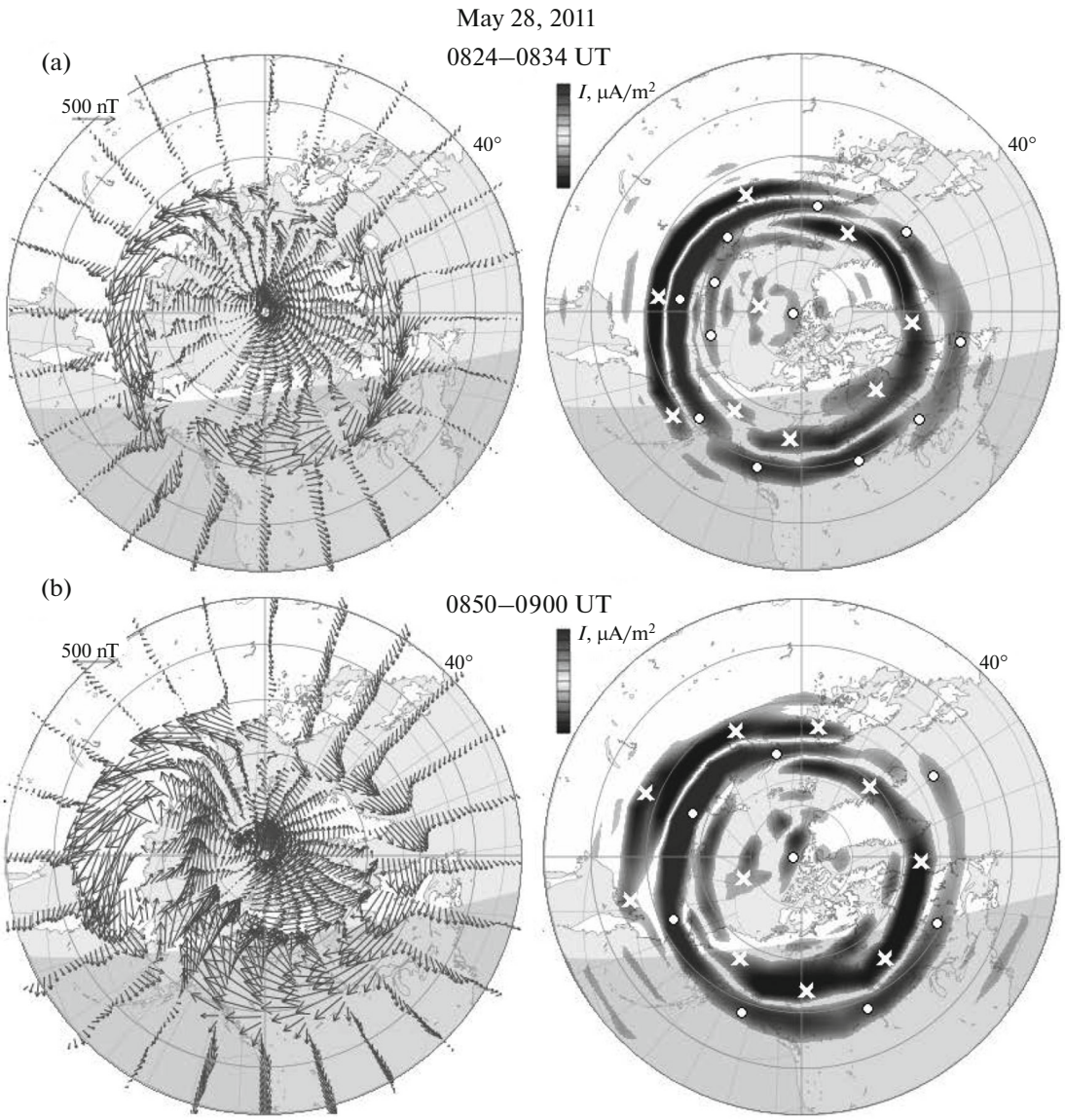

Fig. 3. Maps of the spherical harmonic analysis of magnetic disturbances on May 28, 2011 (left) and maps of the distribution of field-aligned currents (right) according to the AMPERE project data. The upward and downward currents are marked with circles and crosses, respectively. The maps were built in geomagnetic coordinates for the Northern Hemisphere for two time instants: (a) 0820 UT and (b) 0855 UT. Noon (top), midnight (bottom), 06 MLT (right), and 18 MLT (left).

evening sector, an additional downward current of ~15–18 MLT (Fig. 3b) and a huge vortex of disturbances over Eastern Siberia (~16–19 MLT) appeared. This indicates an increase in the eastward electrojet in this region, which may be due to the additional partial ring current that appears in this MLT sector (this will be shown below).

3.3. Ring Current Development during the Supersubstorm

The development of the ring current during the SSS can be assessed with the *SMR* and *SMR_LT* indices, which characterize the ring-current intensity and distribution over the MLT sectors. Figure 4 shows the variations in the *SMR* and *SMR_LT* indices from 0600 to 1300 UT on May 28, 2011. We also add the *SML* index to the figure to compare the dynamics of the ring current and the SSS and add the *MPB* index to estimate the intensity of midlatitude positive bays. The top panel clearly shows the beginning and development of the SSS. The SSS started at ~0805 UT and reached its maximum at ~0850 UT. Below, the variations in the *SMR_LT* ring-current index are shown for four different MLT sectors (night, morning, noon, and evening). Different MLT sectors are shown with

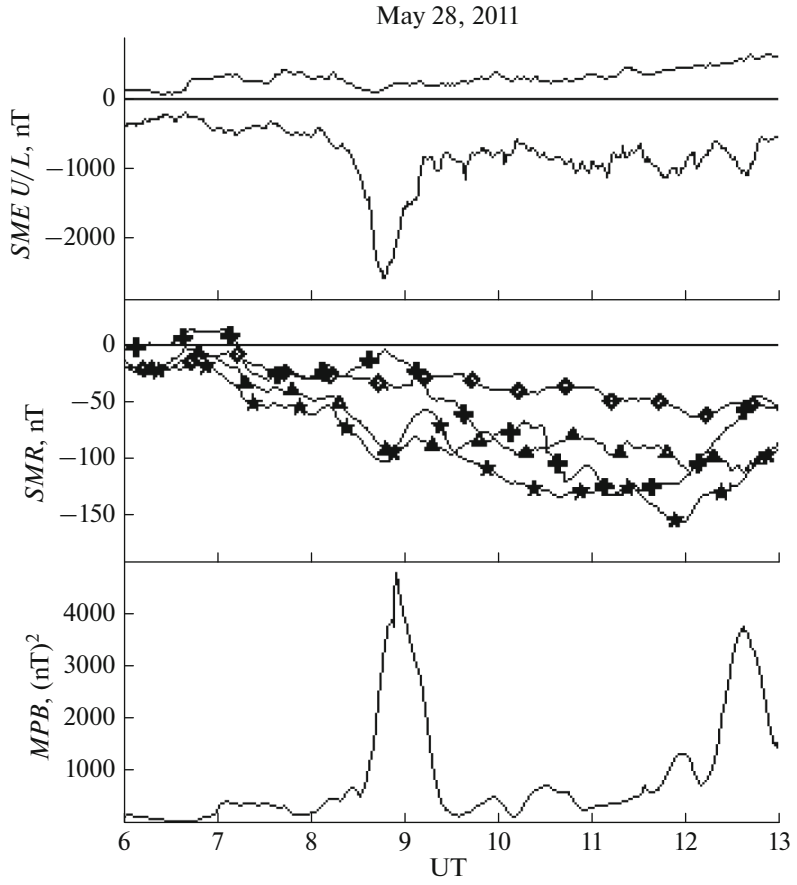

Fig. 4. Variations in *SML*, *SMR_LT*, and *MPB* indices from 0600 to 1300 UT on May 28, 2011. Small symbols on the graphs for the *SMR* index indicate different MLT sectors: *SMR-00* (cross); *SMR-06* (rhombus); *SMR-12* (triangle); and *SMR-18* (asterisk).

different symbols on the *SMR_LT* plots: *SMR_00* (cross), *SMR_06* (rhombus); *SMR_12* (triangle); and *SMR_18* (asterisk).

It can be seen that the ring-current intensity steadily increases, the *SMR* index reaches its minimum values ~−150 nT at around ~11–12 UT, and this occurs in the night, evening, and daytime sectors (*SMR_00*, *SMR_18*, and *SMR_12*). It should be noted that the time ~11–12 UT corresponds to the maximum development of the magnetic storm on May 28, 2011 (Fig. 1). However, the *SMR_12* and *SMR_18* plots show the second additional minimum at around ~0850 UT, which coincides with the minimum in the *SML* index, i.e., it corresponds to the maximum phase of the SSS development. This proves that the ring current increased in the afternoon and evening regions of the magnetosphere during the SSS development.

It can be seen that the minima in the *SML* and *SMR_LT* indices are characterized by a strong burst in the *MPB* index. Thus, at ~0850 UT, a large peak appeared in the *MPB* index with a maximum of ~4000 nT^2, which is associated with strong disturbances at midlatitudes (positive bays). In our event, sufficiently intense positive bays (~100–200 nT) were recorded at stations located in Eastern Siberia, the Far East, Japan, and North America, some of which were presented above (Fig. 2c). It should be noted that these are very large values for both the *MPB* index and the amplitudes of positive bays; their values are several times lower during ordinary substorms (Guineva et al., 2021).

4. DISCUSSION

The supersubstorm observed against the background of the magnetic storm on May 28, 2011, arose under very favorable conditions in the solar wind and IMF: the MC passed by the Earth, a long period of negative values of the IMF B_Z component was observed, and a local pressure jump occurred. In addition, a shock wave (*IS*) was recorded at the end of the SHEATH region at approximately 03 UT (Fig. 1). Therefore, although the appearance of the SSS is associated with the MC of the solar wind rather than its front (SHEATH), this SSS can be attributed to those associated with the development of shock waves. One such event is the SSS observed at the beginning of

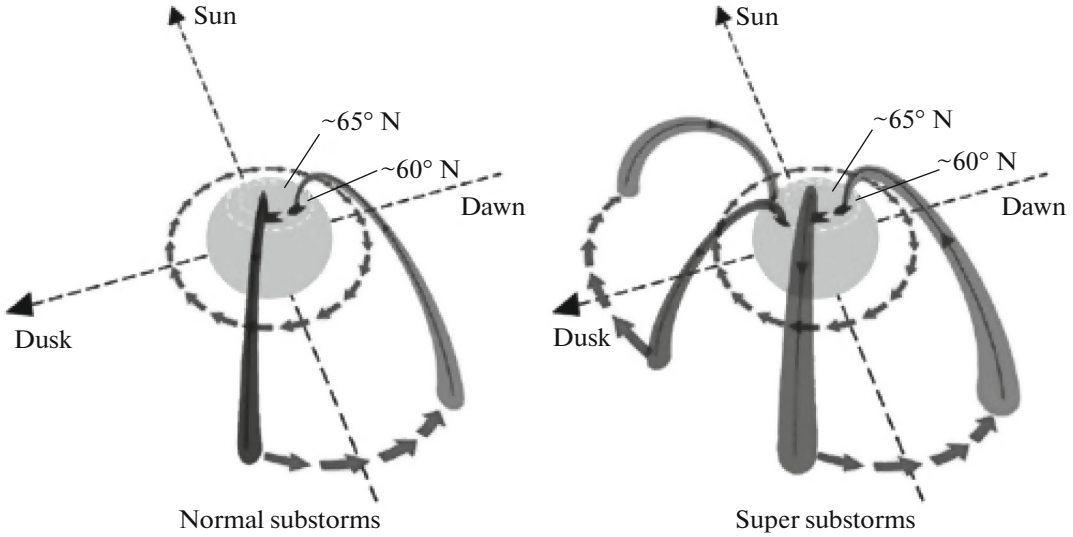

Fig. 5. Substorm current wedge (SCW) model for ordinary substorms (left) and for supersubstorms (right). This figure was taken from Zong et al. (2021).

the storm on April 5, 2010, which has been considered in several studies (Hajra et al., 2018; Nishimura et al., 2020; Zong et al., 2021). Both supersubstorms were isolated, but the SSS on April 5, 2010, consisted of several intensifications, while the event on May 28, 2011, was simpler. It should be noted that the location of magnetic stations during the development of both SSSs was similar: the stations in Alaska and Canada were located in the night sector, the Greenland stations were in the morning sector, the stations of the IMAGE network were in the daytime sector, and the Siberian stations were located in the evening sector (Fig. 2).

Analysis of geomagnetic disturbances showed that the ionospheric currents during the supersubstorm on May 28, 2011, developed on a global scale: from the postmidnight to evening sectors surrounding the Earth. During the SSS development, a very intense, westward electrojet was observed with a maximum in the night sector (~00 MLT), which extended to the noon sector (Figs. 2 and 3). It should be noted that such a global development of the westward electrojet is characteristic of all the SSSs considered earlier (Despirak et al., 2020, 2021).

In addition, as seen from Fig. 3b, the development of the extended westward electrojet was accompanied by a large positive variation in the *N* component of the magnetic field (~200 nT) at geomagnetic latitudes from ~45° to ~55°, which could have led to the observed pulse of the *MPB* index of ~4000 nT^2. It should be noted that the SSS of April 5, 2010, was also accompanied by intense positive bays, and a large burst in the *MPB* index (~6000 nT^2) was observed.

Recent SSS studies (Zong et al., 2021) associated with a shock wave in the solar wind, including the events of April 5, 2010, indicated that during these events an intense, eastward electrojet form on the evening side (~18 MLT). This was assumed to be associated with the amplification of the partial ring current in this MLT sector. A similar amplification of the ring current is also observed in the SSS on May 28, 2011 (Fig. 4). It can be seen that the plots of *SMR_12* and *SMR_18* (partial ring-current indices in the daytime and evening sectors, respectively) contain an additional minimum at around ~0850 UT, which coincides with the minimum in the *SML* index. This indicates that the ring current increased in the afternoon and evening regions of the magnetosphere during the SSS development. This emerging additional ring current closes through field-aligned currents on the eastward electrojet; i.e., it is assumed that an additional current loop (an additional substorm current wedge) appears on the evening side during intense substorms or SSSs (Fu et al., 2021; Zong et al., 2021). This is shown in Fig. 5 taken from Zong et al. (2021), which shows a substorm current wedge (SCW) model observed during normal substorms (left) and an SSS development model (right) consisting of two current wedges, an ordinary wedge (associated with the westward electrojet on the night side) and an additional current wedge (associated with the amplified eastward electrojet and the formation of an additional partial ring current on the evening side). It follows from Figs. 2 and 3 that there was also an increase in the eastward electrojet in the 15–18 MLT sector in our case. During the explosive phase of the SSS, this MLT sector involves an additional downward current, which may be associated with the appearance of the partial ring current (Fig. 4).

The mechanism of the formation of an additional ring current and the acceleration of charged particles

of the ring current during a supersubstorm has not yet been sufficiently studied. Intuitively, it is clear that a huge number of particles can enter the inner magnetosphere during an SSS caused by a shock wave. They can make a significant contribution to the ring current. However, the physical mechanism of this process is still unclear. Several possibilities are discussed in the literature: for example, the energy accumulated in the magnetotail lobes can be released during dynamic pressure pulses, or sudden global magnetospheric compression can induce field-aligned currents that cause ionospheric Joule heating (Tsurutani et al., 2016). Another source could be the plasma waves generated from collisions with a shock wave, which cause the acceleration and precipitation of particles into the magnetosphere (Zong et al., 2012). It was recently shown that fast plasma flows and plasmoids that arise during SSSs contain a large amount of oxygen ions; i.e., calculations should also take into account the contribution of heavy oxygen ions (Zong et al., 2021). Further research is needed for reliable conclusions.

5. CONCLUSIONS

This is a study of planetary geomagnetic disturbances in the main phase of a moderate magnetic storm caused by an interplanetary MC approaching the Earth's magnetosphere during an isolated supersubstorm (SSS) observed on May 28, 2011.

Like those in the SSS cases considered earlier, the ionospheric currents during this SSS developed on a global scale: an intense and extended westward electrojet (with a maximum at around midnight) was observed in the midnight, morning, and daytime sectors, and an intense, eastward electrojet was observed in the afternoon and evening sectors. The development of these global currents was accompanied by intense positive bays, which was reflected by a significant burst in the *MPB* index (~4000 nT^2).

We found that the SSS development was accompanied by a significant increase in the eastward electrojet in the afternoon–evening sector (~15–18 MLT), where an additional, inflowing, longitudinal current appeared. An additional ring current was also concurrently observed in this sector. These facts favor the assumption of an additional substorm current wedge that arose on the evening side during a supersubstorm and closed on the eastward electrojet.

6. ACKNOWLEDGEMENTS

The authors are grateful to the creators of the OMNI database (http://omniweb.gsfc.nasa.gov), the catalog of large-scale solar-wind types (ftp://ftp.iki.rssi.ru/pub/omni/catalog), the SuperMAG database (http://supermag.jhuapl.edu/), IMAGE (http://space.fmi.fi/image/), and AMPERE (http://www.ampere.jhuapl.edu) for the permission to use these data in the study.

FUNDING

The work by I.V. Despirak, N.G. Kleimenova, A.A. Lyubchich, and P.V. Setsko was supported by the Russian Foundation for Basic Research, project no. 20-55-18003Bolg_a; the work by R. Werner was supported by the National Science Foundation of Bulgaria, project no. KP-06-Russia/15); and the work by L.I. Gromova was conducted within the state task of the Pushkov Institute of Terrestrial Magnetism and Radiowave Propagation, Russian Academy of Sciences.

CONFLICT OF INTEREST

The authors declare that they have no conflicts of interest.

REFERENCES

Akasofu, S.-I., The development of the auroral substorm, *Planet. Space Sci.*, 1964, vol. 12, no. 4, pp. 273–282. https://doi.org/10.1016/0032-0633(64)90151-5

Chu, X., Hsu, T.-S., McPherron, R.L., Angelopoulos, V., Pu, Z., Weygang, J.J., Khuhara, K., Connors, M., Kissenger, J., Zhang, H., and Amm, O., Development and validation of inversion technique for substorm current wedge using ground magnetic field data, *J. Geophys. Res.: Space Phys.*, 2014, vol. 119, pp. 1909–1924. https://doi.org/10.1002/2013ja019185

Chu, X., McPherron, R.L., Hsu, T.-S., and Angelopoulos, V., Solar cycle dependence of substorm occurrence and duration: Implications for onset, *J. Geophys. Res.*: *Space Phys.*, 2015, vol. 120, pp. 2808–2818. https://doi.org/10.1002/2015JA021104

Connors, M., McPherron, R.L., Anderson, B.J., Korth, H., Russell, C.T., and Chu, X., Electric currents of a substorm current wedge on 24 February 2010, *Geophys. Res. Lett.*, 2014, vol. 41, pp. 4449–4455. https://doi.org/10.1002/2014gl060604

Despirak, I.V., Lyubchich, A.A., and Kleimenova, N.G., Supersubstorms and conditions in the solar wind, *Geomagn. Aeron. (Engl. Transl.)*, 2019, vol. 59, no. 2, pp. 170–176. https://doi.org/10.1134/S0016793219020075

Despirak, I.V., Kleimenova, N.G., Gromova, L.I., Gromov, S.V., and Malysheva, L.M., Supersubstorms during storms of September 7–8, 2017, *Geomagn. Aeron. (Engl. Transl.)*, 2020a, vol. 60, no. 3, pp. 292–300. https://doi.org/10.1134/S0016793220030044

Despirak, I.V., Lubchich, A.A., and Kleimenova, N.G., Several special conditions in the solar wind for a supersubstorm appearance. *Physics of auroral phenomena*, *Proc. XLIII Annual Seminar*, Apatity, 2020b, pp. 7–10. https://doi.org/10.37614/2588-0039.2020.43.001

Despirak, I.V., Lyubchich, A.A., Kleimenova, N.G., Gromova, L.I., Gromov, S.V., and Malysheva, L.M., Longitude geomagnetic effects of the supersubstorms during the magnetic storm of March 9, 2012, *Bull. Russ. Acad. Sci.: Phys.*, 2021, vol. 85, no. 3, pp. 246–251. https://doi.org/10.3103/S1062873821030096

Feldstein, Y.I. and Starkov, G.V., Dynamics of auroral belt and geomagnetic disturbances, *Planet. Space Sci.*, 1967, vol. 15, pp. 209–229.

Feldstein, Y.I., Popov, V.A., Cumnock, J.A., Prigancova, A., Blomberg, L.G., Kozyra, J.U., Tsurutani, B.T., Gromova, L.I., and Levitin, A.E., Auroral electrojets and boundaries of plasma domains in the magnetosphere during magnetically disturbed intervals, *Ann. Geophys.*, 2006, vol. 24, pp. 2243–2276. https://doi.org/10.5194/angeo-24-2243-2006

Fu, H., Yue, C., Zong, Q.-G., Zhou, X.-Z., and Fu, S., Statistical characteristics of substorms with different intensity, *J. Geophys. Res.: Space Phys.*, 2021, vol. 126, p. e2021JA029318. https://doi.org/10.1029/2021JA029318

Gjerloev, J.W., A global ground-based magnetometer initiative, *Eos Trans. Am. Geophys. Union*, 2009, vol. 90, pp. 230–231. https://doi.org/10.1029/2009EO270002

Gjerloev, J.W., The SuperMAG data processing technique, *J. Geophys. Res.*, 2012, vol. 117, A09213. https://doi.org/10.1029/2012JA017683

Guineva, V., Werner, R., Despirak, I., Bojilova, R., and Raykova, L., Mid-latitude positive bays during substorms by quiet and disturbed conditions, *C. R. Acad. Bulg. Sci.: Space Phys.*, vol. 74, pp. 1185–1193. https://doi.org/10.7546/CRABS.2021.08.10

Hajra, R. and Tsurutani, B.T., Interplanetary shocks inducing magnetospheric supersubstorms (SML < –2500 nT): Unusual auroral morphologies and energy flow, *Astrophys. J.*, 2018, vol. 858, no. 2, p. 123. https://doi.org/10.3847/1538-4357/aabaed

Hajra, R., Tsurutani, B.T., Echer, E., Gonzalez, W.D., and Gjerloev, J.W., Supersubstorms (SML < –2500 nT): Magnetic storm and solar cycle dependences, *J. Geophys. Res.: Space Phys.*, 2016, vol. 121, pp. 7805–7816. https://doi.org/10.1002/2015JA021835

McPherron, R.L. and Chu, X., The midlatitude positive bay index and the statistics of substorm occurrence, *J. Geophys. Res.*: *Space Phys.*, 2017, vol. 123, pp. 2831–2850. https://doi.org/10.1002/2017JA024766

McPherron, R.L., Russell, C.T., and Aubry, M.P., Satellite studies of magnetospheric substorms on August 15, 1968: 9. Phenomenological model for substorms, *J. Geophys. Res.*, 1973, vol. 78, no. 16, pp. 3131–3149. https://doi.org/10.1029/ja078i016p03131

Meng, C.-I. and Akasofu, S.-I., A study of polar magnetic substorms: 2. Three-dimensional current system, *J. Geophys. Res.*, 1969, vol. 74, no. 16, pp. 4035–4053. https://doi.org/10.1029/ja074i016p04035

Newell, P.T. and Gjerloev, J.W., Substorm and magnetosphere characteristic scales inferred from the SuperMAG auroral electrojet indices, *J. Geophys. Res.*, 2011b, vol. 116, no. A12, p. A12232. https://doi.org/10.1029/2011JA016936

Nishimura, Y., Lyons, L.R., Gabrielse, C., Sivadas, N., Donovan, E.F., Varney, R.H., Angelopoulos, V., Weygand, J.M., Conde, M.G., and Zhang, S.R., *J. Geophys. Res.: Space Phys.*, 2020, vol. 125, no. 4, p. e2019JA027654. https://doi.org/10.1029/2019JA027654

Rostoker, G., Macrostructure of geomagnetic bays, *J. Geophys. Res.*, 1968, vol. 73, no. 13, pp. 4217–4229. https://doi.org/10.1029/ja073i013p04217

Sergeev, V.A., Tsyganenko, N.A., Smirnov, M.V., Nikolaev, A.V., Singer, H.J., and Baumjohann, W., Magnetic effects of the substorm current wedge in a "spread-out-wire" model and their comparison with ground, geosynchronous, and tail lobe data, *J. Geophys. Res.*, 2011, vol. 116, p. A07218. https://doi.org/10.1029/2011JA016471

Troshichev, O.A., Podorozhkina, N.A., Sormakov, D.A., and Janzhura, A.S., *PC* index as a proxy of the solar wind energy that entered into the magnetosphere: Development of magnetic substorms, *J. Geophys. Res.: Space Phys.*, 2014, vol. 119, no. 8, pp. 6521–6540. https://doi.org/10.1002/2014JA019940

Tsurutani, B.T., Hajra, R., Echer, E., and Gjerloev, J.W., Extremely intense (SML ≤ –2500 nT) substorms: Isolated events that are externally triggered?, *Ann. Geophys.*, 2015, vol. 33, no. 5, pp. 519–524. https://doi.org/10.5194/angeocom-33-519-2015

Tsurutani, B.T., Hajra, R., Tanimori, T., Takada, A., Remya, B., Mannucci, A.J., Lakhina, G.S., Kozyra, J.U., Shiokawa, K., Lee, L.C., Echer, E., Reddy, R.V., and Gonzales, W.D., Heliospheric plasma sheet (HPS) impingement onto the magnetosphere as a cause of relativistic electron dropouts (REDs) via coherent EMIC wave scattering with possible consequences for climate change mechanisms, *J. Geophys. Res.: Space Phys.*, 2016, vol. 121, no. 10, pp. 10130–10156. https://doi.org/10.1002/2016JA022499

Viljanen, A. and Häkkinen, L., IMAGE magnetometer network, in *Satellite–Ground Based Coordination Sourcebook*, Lockwood, M., Wild, M.N., and Opgenoorth, H.J., Eds., ESA, 1997, pp. 111–117.

Zong, Q.-G., Wang, Y.F., Zhang, H., Fu, S.Y., Zhang, H., Wang, C.R., Yuan, C.J., and Vogiatzis, I., Fast acceleration of inner magnetospheric hydrogen and oxygen ions by shock induced ULF waves, *J. Geophys. Res.*, 2012, vol. 117, no. A11, p. A11206. https://doi.org/10.1029/2012JA018024

Zong, Q.-G., Yue, C., and Fu, S.-Y., Shock induced strong substorms and super substorms: Preconditions and associated oxygen ion dynamics, *Space Sci. Rev.*, 2021, vol. 217, no. 33. https://doi.org/10.1007/s11214-021-00806-x

Translated by V. Arutyunyan